The thesis committee for Patrick Ponath

certifies that this is the approved version of the following thesis:

Construction and Assembly of a Scanning Tunneling Microscope

APPROVED BY

SUPERVISING COMMITTEE:

Supervisor: _____

Alex de Lozanne

Co-Supervisor: _____

Alex Demkov

Construction and Assembly of a Scanning Tunneling Microscope

by

Patrick Ponath, B.S.

Thesis

Presented to the Faculty of the Graduate School

of the University of Texas at Austin

in Partial Fulfillment

of the Requirements

for the Degree of

Master of Arts

The University of Texas at Austin

August 2011

Acknowledgments

First and foremost I want to thank my professor Alex de Lozanne, for the opportunity to accomplish my master thesis in his lab. Furthermore I would like to thank him, for the support I've received during the whole year. I benefited a lot of his experience and his practical tips.

Special thanks go to our post-doc Dr. Seong Heon Kim, who instructed me with the assembly of the STM. Moreover I'm very thankful to all of his hints he gave me and the time he took to explain me the basics of scanning tunneling microscopy.

I would also like to thank Jack Clifford who instructed me in the machine shop and who gave me very useful tips for the machining of the STM parts in the student machine shop.

Furthermore I have to thank Leu-Jen Chen who always had a sympathetic ear if I had problems with the electronics.

I would also like to thank the other students Morgann Berg, Neliza Léon-Brito and Ryan Jaehne for their support, hints and interesting conversations.

Finally I would like to thank professor Demkov who proof-read my thesis.

Construction and Assembly of a Scanning Tunneling Microscope

by

Patrick Ponath, M.A.
The University of Texas at Austin, 2011
Supervisor: Alex de Lozanne
Co-Supervisor: Alex Demkov

In the scope of this master thesis, a home-made brass scanning tunneling microscope (STM) was machined, assembled and tested for its functionality. For this microscope, a new approach-technique was used which follows the design suggested by Pan. The difference to Pan's design is the use of piezoplates, instead of piezostacks. Hence, the approach is still based on the stick and slip motion, but it allows the microscope to be more compact. A new and simple electronic circuit, in order to control the approach, is presented and was put together. This circuit is based on mechanical relays, which provide a sufficient long time gap between the single moving steps, due to their mechanical functional principle. Subsequently the approach-technique and the scanning was successfully tested. Finally, first images of HOPG were taken under ambient conditions.

Contents

List of Figures

1 Introduction

During the last century, physics, in particular solid state physics, was subject to a remarkable development. A milestone was definitely the development of quantum mechanics in the beginning of the 20^{th} century, which allowed the description of matter on an atomic level. However, scientists were stretched to their limits soon, since for some physical phenomenas, several, partially strongly contradictory theories, could have applied.
A famous example is the real structure of the unit cell of silicon, which has been unknown for quite a long time. Heated discussions were led, which resulted in several suggestions for the unit cell structure of silicon.
Binnig and Rohrer were the first who could celebrate the breakthrough of having observed the 7×7 reconstruction of a Si(111) surface in 1983 [1]. Consequently they were rewarded with the Nobel Price in 1986 for this observation. Beforehand, Binnig and Rohrer have successfully experimented with tunneling currents [2] for a couple of years, until they were able to develop a scanning tunneling microscope (STM) in 1982 [3], [4]. This invention became a wide-spread technique in surface science and initiated a boom in the research and advancement of scanning tunneling microscopy.

The STM is based on a tunneling current, which is a quantum mechanical effect. This tunneling current occurs, when a metallic tip is brought close enough to an electrically conductive sample held at a different potential.
The tunneling current though, varies with the distance to the surface of the sample, what is utilized by the STM, as the change of current, while rastering the surface, can be used to create a topography of the surface.

Hence, the STM is suitable to scan surfaces without damaging them. Nevertheless

the STM is narrowed to only metallic or electric conductive samples, which restricts its applicability. As a consequence, Binnig developed the atomic force microscope (AFM), which utilizes the force between cantilever and sample to scan the surface [5]. Its advantage is based on being able to scan even insulating samples, since the principle is independent of electric conductivity, which can, for instance, be used to observe dynamic processes in living cells [6].

But apart from imaging surfaces, the STM depicts a good method for atom manipulation nowadays as well, as shown by Meyer [7], Eigler and Schweizer [8],[9]. In 1990 Eigler and Schweizer succeeded the repositioning of Xe-atoms on a nickel (110) surface (image 1) for the first time.

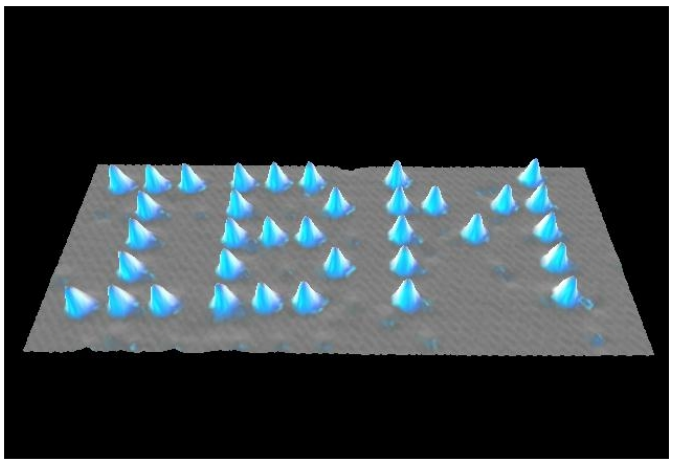

fig. 1: Xenon atoms on a Ni(110) surface, done originally by IBM Corporation [10].

In the scope of this master thesis, an STM with a new approach design was machined and assembled. The approach system being used for this STM is a modified version of Pan's idea of moving the scanner tube [11] and was subsequently tested for its functionality. Furthermore the functionality of the whole STM was tested by taking images of HOPG under ambient conditions.

2 Theoretical background

2.1 Principles of the tunneling effect

As the name already implies, an STM makes use of a tunneling current and hence one has to take quantum theory into account.

In classical mechanics, as generally known, an electron can't reach regions behind a potential barrier of a quantum well, if the potential is higher than the total energy of the electron. In quantum mechanics though, the electron has a nonzero probability to be found behind the potential barrier although the potential might exceed the total energy of the electron. A scanning tunneling microscope makes use of this effect.

If the metallic tip of the microscope is brought close enough to the sample and a voltage is applied between them, a tunneling current occurs. Both, the vacuum (or air) which is in between the tip and the sample and the workfunction of the material, act as the potential barrier. For reasons of simplifications one can use a one-dimensional model to describe the physics of an STM.

In the following the theory of the working principle of an STM will be described. Starting from the stationary Schroedinger-equation:

$$-\frac{\hbar^2}{2m}\frac{d^2}{dz^2}\psi(z) + U(z)\psi(z) = E\psi(z) \tag{1}$$

whereby m depicts the electron mass, $\psi(z)$ the wavefunction of the electron, U(z) the potential and E the eigenenergy, one obtains:

$$\psi(z) = \psi(0)e^{-\kappa z} \tag{2}$$

as a solution for the electron wavefunction in the forbidden region of a quantum well. κ is the decay constant and is defined as follows:

$$\kappa = \frac{\sqrt{2m(U-E)}}{\hbar} \tag{3}$$

Hence the probability to find the electron in the forbidden region can be determined as $|\psi(0)|^2 e^{-2\kappa z}$ which has a nonzero value. Therefore the electron has a certain probability to tunnel through a potential barrier.

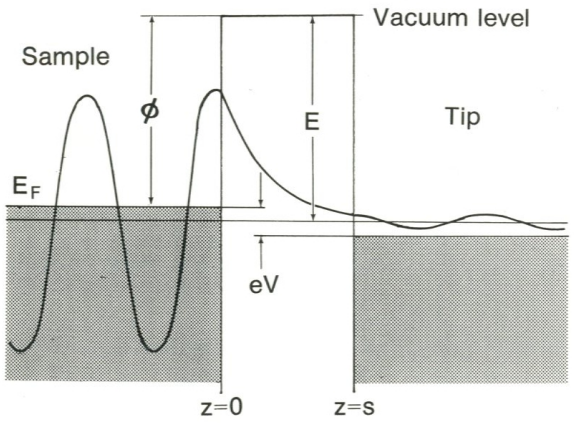

fig. 2: A voltage V is applied between the tip and the sample which increases the Fermi energy of the sample in the order of several eV. This eventually leads to a tunneling current from the sample to the tip if both are close enough.[12]

Figure 2 shows a one-dimensional metal-vacuum-metal tunneling junction which applies to the conditions of an STM between the tip and the sample. The work function ϕ depicts the potential barrier which varies with the used metal and must be overcome by the electron. For reasons of simplification one assumes the Fermi energy E_F as the upper energy for the electrons in a metal, although it only applies for electrons at a temperature of T=0 K.

If the used tip and sample are from the same material and are brought close together, a tunneling current occurs. But without applying a voltage, electrons from both sides tunnel through the barrier with the same probability, wherefore the net tunneling current is zero. However, by applying a bias voltage V between the tip and the sample one can achieve a net tunneling current into one direction.

This feature is also illustrated in figure 2 where electrons with a state ψ_n and an energy of E_n, lying between E_F-eV and E_F, can tunnel from the sample into the tip. Furthermore if eV$<<$ ϕ then $E_n \approx -\phi$, because at low temperatures all the electrons are close to the Fermi energy. As a consequence one can determine an approximation for the probability w for an electron at the tip at z=W in the nth state:

$$w \propto |\psi_n(0)|^2 e^{-2\kappa W} \tag{4}$$

where $\psi_n(0)$ is the value of the wavefunction at the sample surface and

$$\kappa = \frac{\sqrt{2m\phi}}{\hbar}. \tag{5}$$

For that reason it is intelligible that the tunneling current depends on the number of electronic states on the surface of the sample within the energy level E_F and E_F-eV. Now the tunneling current I can be written as

$$I \propto \sum_{E_n=E_F-eV}^{E_F} |\psi_n(0)|^2 e^{-2\kappa W} \tag{6}$$

By assuming a bias voltage V which is small enough that the density of states is almost not affected, an approximation can be done. The sum in equation 6 can be replaced by the local density of states (LDOS) which is defined as follows:

$$\rho_S(z, E) = \frac{1}{\epsilon} \sum_{E_n=E_F-eV}^{E_F} |\psi_n(z)|^2 \tag{7}$$

if the energy interval ϵ is sufficiently small. The local density of states is generally defined as the number of electrons per unit energy and volume.
By using equations 2 and 7 the tunneling current can be expressed with the density of states as

$$I \propto \rho_S(0, E_F) e^{-2\kappa W} \tag{8}$$

which can be approximated as

$$I \approx V \rho_s(0, E_F) e^{-1.025\sqrt{\phi} W} \tag{9}$$

A typical value for the work function strongly depends on the metal but usually it lies between 2-5 eV. If one assumes a work function of $\phi = 4.5$ eV, which applies for example for tungsten [13], the tunneling current increases about a magnitude if the tip approaches the sample approximately for one $\mathring{A}$.
However, equation 9 also illustrates that the tunneling current and thus the image taken by an STM is not an image of the atoms themselves but rather the local electron density of the surface of the sample at the Fermi energy. This means that an STM can be used for spatially-resolved tunneling spectroscopy (STS).

2.2 Spatially-resolved tunneling spectroscopy

The first scientist who could present a theoretically derived description of a tunneling current through a metal-insulator-metal (MIM) junction was Bardeen. He made use of a time-dependent perturbation approach, which is simple enough to describe the physics of many experiments. Bardeen made the Ansatz to split up the system into two separate subsystems (tip and sample). Instead of solving the Schroedinger equation for the combined tip-sample system, he used the stationary Schroedinger equation for the two subsystem to calculate the electronic states in tip and sample (image 3).

The overlap integral of the wavefunction from tip and sample which had to be calculated can be described by a tunneling matrix element M [14]:

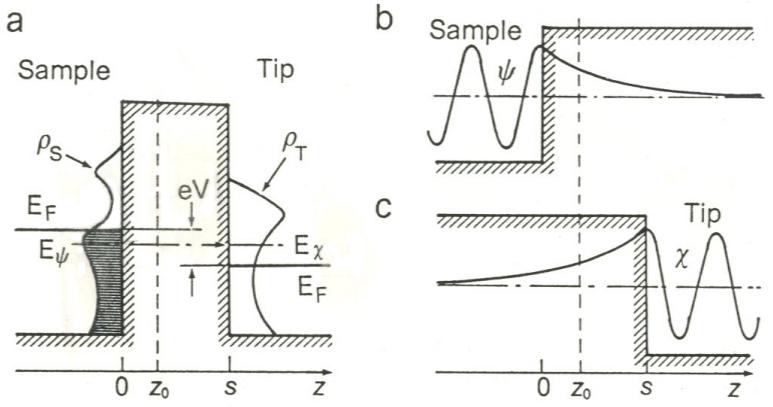

fig. 3: Image a illustrates the energies which apply to the real tip-vaccum-sample system. Images b and c illustrate an approximation of the two decoupled systems (tip and sample), for which Bardeen solved the Schroedinger equation separately.[12]

$$M = \frac{\hbar}{2m} \int_{z=z_0} \left(\chi^* \frac{\partial \psi}{\partial z} - \psi \frac{\partial \chi^*}{\partial z} \right) dS \tag{10}$$

M describes the transition of electrons from the tip to the sample. ψ and χ are the wavefunctions of the electrons in tip and sample, respectively. By using Fermi's golden rule, the probability W of an electron tunneling from a state ψ with energy E_ψ to a state χ with energy E_χ can be calculated:

$$W = \frac{2\pi}{\hbar} |M|^2 \delta(E_\psi - E_\chi) \tag{11}$$

A delta function is used due to the energy conservation law, since the electrons can only tunnel into states with the same energy level. With this result, the tunneling current can be calculated by summing over all possible electronic states:

$$I = \frac{4\pi e}{\hbar} \int_{-\infty}^{\infty} [f(E_F - eV + \epsilon) - f(E_F + \epsilon)] \times \rho_S(E_F - eV + \epsilon)\rho_T(E_F + \epsilon)|M|^2 d\epsilon \tag{12}$$

Hereby f(E) is the Fermi distribution function, since we are dealing with electrons. ρ_S and ρ_T correspond to the density of states of tip and sample. Although equation 12 is the general formula to describe the tunneling current between tip and sample, it can be further approximated. For measurements in low temperature areas one can assume that $k_B T$ is much smaller than $E\text{-}E_F$. As a result the Fermi distribution functions can be approximated as step functions which changes the limits of the integral:

$$I = \frac{4\pi e}{\hbar} \int_{0}^{eV} \rho_S(E_F - eV + \epsilon)\rho_t(E_F + \epsilon)|M|^2 d\epsilon \tag{13}$$

Finally a last approximation can be made by assuming that the tunneling matrix M doesn't change appreciably in the small energy interval between 0 and eV. In this case one can assume M as a constant, which leads to the Bardeen formula:

$$I \propto \int_{0}^{eV} \rho_S(E_F - eV + \epsilon)\rho_T(E_F + \epsilon) d\epsilon \tag{14}$$

This result is fairly remarkable, because the above equation means that the tunneling current is only dependent on the density of states from the tip and sample. Both, the tip and the sample, contribute equally to the tunneling current. One can make use of this result by using a tip with a constant density of states or simply a free-electron tip, in order to measure the local density of states of a sample. If ρ_T is a constant, then the tunneling current only depends on the density of states of the sample:

$$\frac{dI}{dV} \propto \rho_S(E_F - eV) \tag{15}$$

Thus STS provides a good method to measure one of the most important properties of a material, the LDOS.

2.3 The s-wave tip model

Ideally the tip which tapers, exhibits only one atom at its peak. In practice though, this shape of a tip can never be achieved. As an approximation the s-wave tip model was introduced by Tersoff and Hamann [15] in 1983. In their work, they didn't assume a perfect tip with only one atom, but a taper tip with a radius of curvature R, as can be seen in image 4. One can consider this as a spherical quantum well with radius R where the solution of this well depict the wavefunctions of the tip. But if one only assumes the s-wavefunctions as crucial, the tunneling current simplifies and is proportional to the LDOS in the center of the tip $\vec{r_0}$ [15] at low bias:

$$I \propto \sum_{E_\mu = E_F - eV}^{E_F} |\psi_\mu(\vec{r_0})|^2 = eV\rho_S(\vec{r_0}, E_F) \tag{16}$$

This makes the constant-current STM image independent of the tip properties, because it only depends on the applied voltage and the LDOS of the sample. Thus the image only reflects the properties of the scanned sample.

Furthermore Tersoff and Hamann showed for metals with a periodicity a, that the corrugation amplitude z of the Fermi-level LDOS can be written as [12][16]:

$$\Delta z = \frac{2}{\kappa} exp\left[-2\left(\sqrt{\kappa^2 + \frac{\pi^2}{a^2}} - \kappa\right) z\right] \tag{17}$$

where z is the distance between the sample surface and the center of the curvature of the tip and $\kappa = \frac{\sqrt{2m\phi}}{\hbar}$ is the minimum inverse decay length for the wavefunction in vacuum. ϕ depicts the work function of the used material.

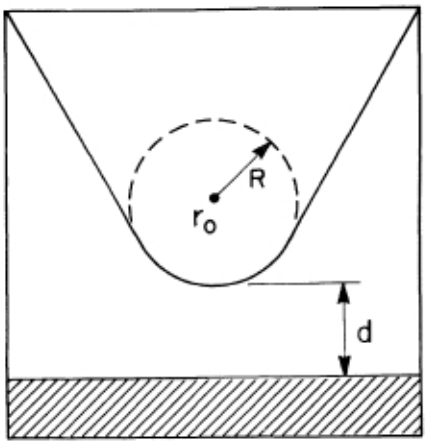

fig. 4: The s-wave tip model: The tip with a radius of curvature R is considered as a spherical quantum well, but only the s-wave solutions are used for the tip wavefunction [15].

It turns out, that for a large periodicity a>> $\frac{\pi}{\kappa}$ the corrugation amplitude can be approximated by:

$$\Delta z = const * exp\left(-\frac{\pi^2 z}{a^2 \kappa}\right) \tag{18}$$

This approximation coincides with other theoretical predictions which were published beforehand. In 1984 Stoll derived a formula which also describes the gap between tip and sample. However, this equation is only valid for a large periodicity "a" of the sample's surface structure (a>> $\frac{\pi}{\kappa}$) and a large gap "d" (d >> $\frac{2}{\kappa}$) between the tip and the surface of the sample and reads as follows [17]:

$$\frac{\Delta d}{h_S} = exp\left(-\frac{\pi^2 (R+d)}{\kappa a^2}\right) \tag{19}$$

Hereby h_S depicts the amplitude of the surface and κ is the decay constant which was introduced in equation 3. Since the radius R of the curvature of the tip is a constant, it becomes irrelevant. Therefore the equation can be written as:

$$\frac{\Delta d}{h_S} = const * exp\left(-\frac{\pi^2 d}{\kappa a^2}\right) \tag{20}$$

and one can see the coincidence with the formula derived from Tersoff and Hamann.

3 STM components, approach and scanning mechanism

In general an STM consists of several parts, but it can be reduced to three basic components.
The first one involves the mechanical parts of the microscope. The second component is responsible for the motion of the scanner tube in 3 axes and the last one can be summarized as the electronics to create the feedback loop, which is necessary to run the STM in the constant current mode. Apart from that, the data acquisition is another component, which is necessary for taking images.
In the following all the components will be described in detail.

3.1 The mechanical parts

Within the scope of this thesis, an STM was constructed and assembled which exhibits a very compact design. The used material for the STM is brass, since it is on the one hand rigid enough to achieve some high quality images but on the other hand not too difficult to machine. However, this allows the STM to be operated only in HV.
The machined pieces are 6 legs, one body, one tube for the scanner tube and the sample holder. In the following I will describe each part of the STM, which was constructed in the machine shop, in detail:

3.1.1 T-leg

In order to construct a very compact design of an STM, two different types of legs had to be constructed. One type had the shape of a T and can be seen in image 5 (length: 1.5625”, total width: 0.6000”, height: 0.1950”). In this image one can see that the T-leg has 4 holes. 3 of them, the 2 bottom ones and the one at the top, will be used to screw the leg into the body. The 4th hole serves as an electrical

connection for the piezoplate which will be attached to the leg.

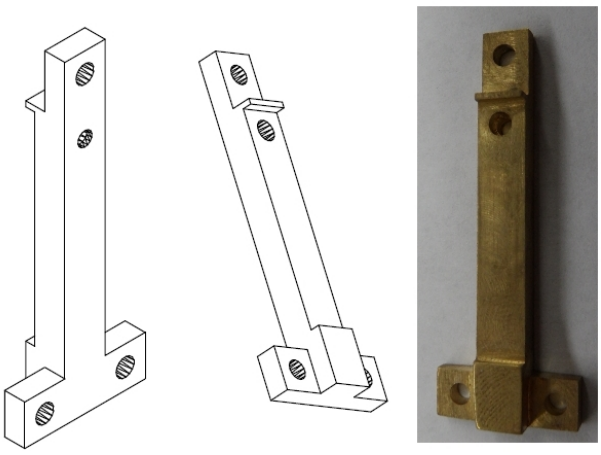

fig. 5: Draft of the T-shaped legs [18].

However, the assembly of the microscope will be explained in detail in section 4. All in all 4 T-legs had to be constructed.

3.1.2 I-leg

The other type of leg has the shape of an I (Image 6, length: 1.5625”, width: 0.2000”, height: 0.1925”).

The main difference between the I- and the T-leg is, apart from the shape, a deep cut underneath the top hole. This cut is essential, because it allows the loose part of the leg to be bent, while the other part is screwed to the body. By the help of a spring one can push the loose part against the tube and consequently adjust the pressure exerted on the scanner tube.

These springs were machined out of beryllium-copper and exhibit two holes, in order to screw them into the body. They can be seen in image 10.

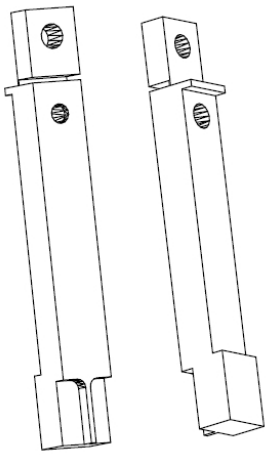

fig. 6: Draft of the I-shaped legs [18].

3.1.3 Body

The body of the microscope has the shape of a hollow cylinder (height: 2.29”, outer diameter: 1.00”, inner diameter: 0.4375”) with 6 milling grooves at the outer surface for the 4 T- and 2 I-legs (Image 7).

The legs are used to move the scanner tube which will be placed in the center of the body what can be seen in image 7b). In order to screw the legs into the body, 3 tapped holes were drilled in the milling grooves. Furthermore, 3 through holes were drilled at the top of the body to attach the sample holder.

3.1.4 Tube

The tube is a hollow cylinder (length: 1.8650”, outer diameter: 0.380”, inner diameter: 0.290”) and is flattened on 6 sides in order to avoid contact with the piezoplates which will lay on this position. Furthermore there are 6 little milling grooves, alternately on opposite sides at the end of the flattened surfaces to attach little boron nitride pads which are necessary for the walking process.
The tube has the shape of a hollow cylinder, because the piezotube which is re-

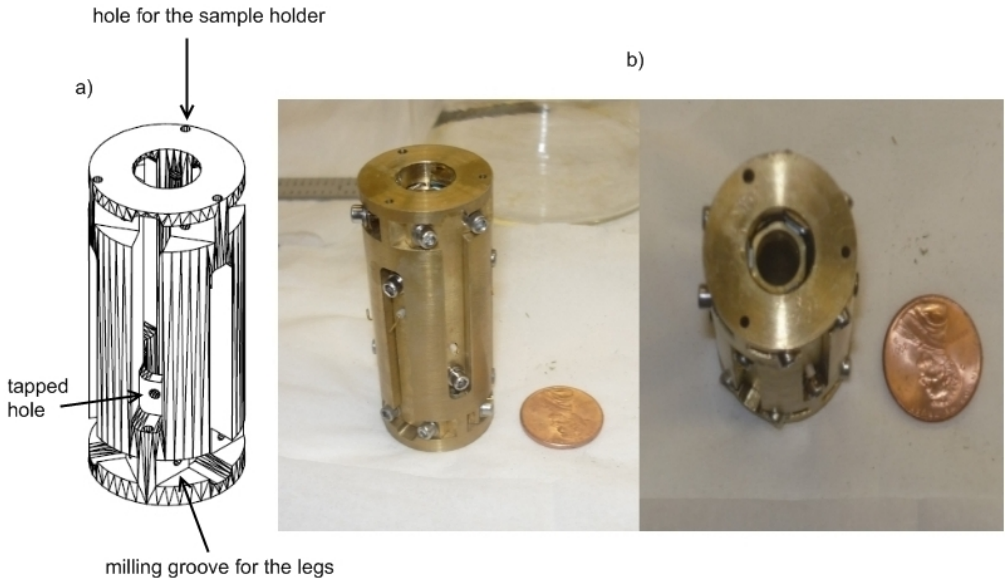

fig. 7: Image a) shows the draft of the body. The milling grooves where the legs will be screwed in are clearly visible. Image b) shows the entire and already assembled body with the legs and scanner tube. To illustrate the compactness of the microscope a 1 cent coin was put next to it [18].

sponsible for the fine movement in 3 axis will be put inside.

3.1.5 Sample holder

For the microscope, a simple sample holder was constructed (image 9). It has a round shape and 3 drilled through holes from the top to the bottom. These holes have the exact same distance as the 3 holes on top of the body, in order to connect the body with the sample holder by using 3 straight alumina sticks. The side, where the sample will be placed, was flattened to achieve an almost rectangular tip-sample system later. Apart from that, three tapped holes were drilled laterally which end in the holes which were drilled vertically. The purpose of these tapped holes is to use screws to tighten the sample holder to the 3 alumina sticks to adjust

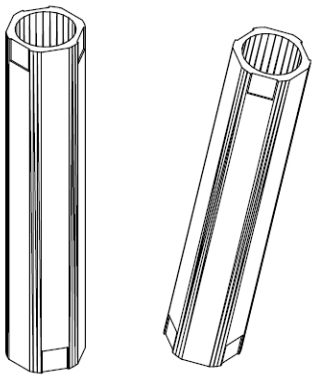

fig. 8: Draft of the brass tube [18].

the correct height for the sample. As one can see in image 9 two beryllium copper clips were glued to the sample holder with silver epoxy. Silver epoxy is electrically conductive, wherefore the clips serve on one side to hold the sample tight in place, but on the other side to have an electrical connection.

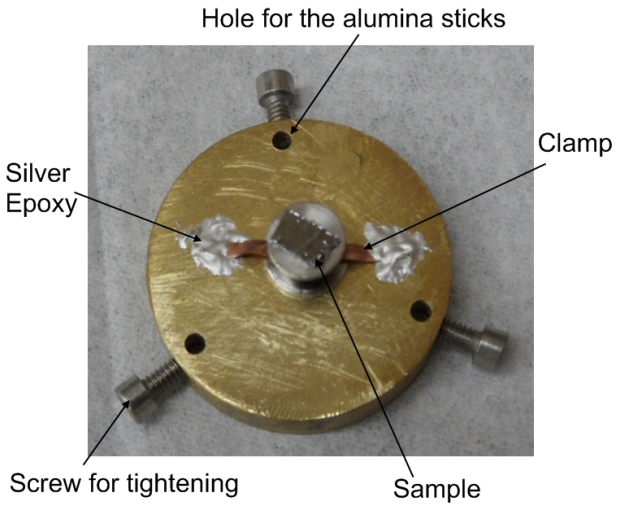

fig. 9: Sample holder with a graphite sample.

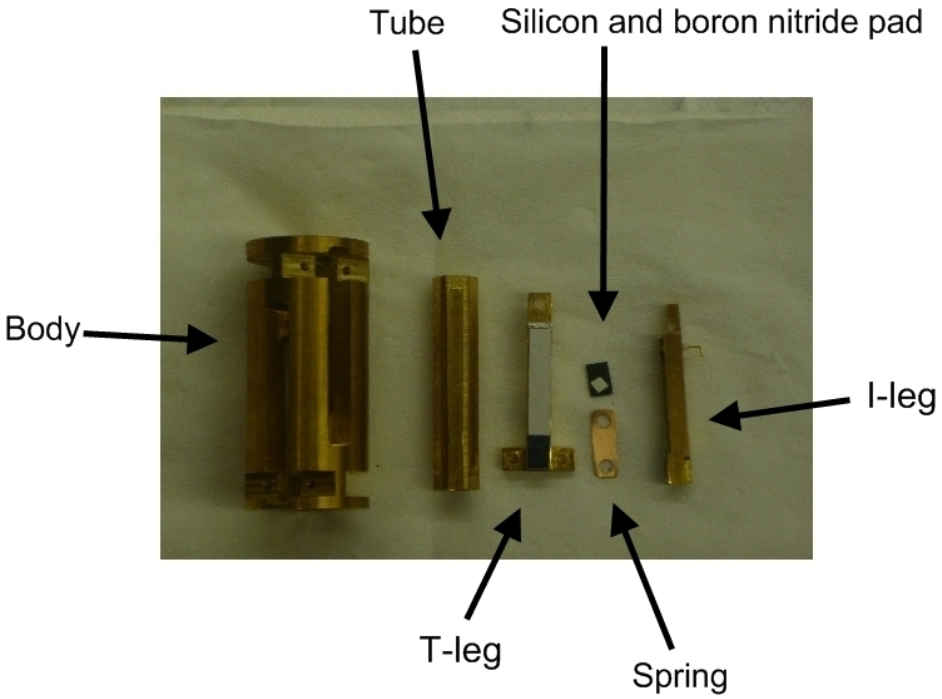

fig. 10: This image shows all the pieces which were constructed in the machine shop (except of the sample holder). Furthermore one can see the white boron nitride pad lying on top of a little silicon pad.

3.2 Motion in 3 axes

3.2.1 Piezoceramic actuator

One of the most crucial parts of an STM is the piezoelectric tube, because it is responsible for the fine motion in 3 axis and the correct positioning and controlling of the tip, in order to scan the surface of the sample. Ideally one wants to use a highly accurate approach system which can move the tip sometimes in even less than nanometer steps both in the x-y- and z-direction, since the usual gap distance between the tip and the sample is only in the order of a few nanometers. The range of the x-y-direction though, can be in the μm range.

A commonly used solution to approach and move the tip is a piezoelectric actuator, because it is rigid enough to compensate vibrations and it expands linearly with an applied voltage.

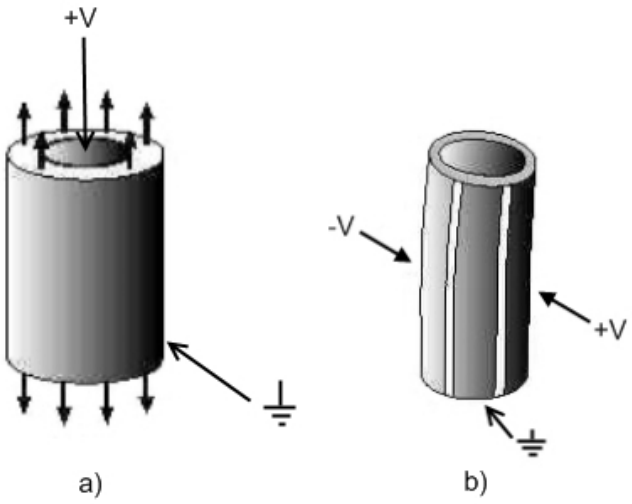

fig. 11: a) By only applying a voltage to the inner electrode, while the outer electrodes are grounded, the tube expands into the z-direction. b) Applying a voltage ±V to two opposite outer electrodes though, while the other electrodes are grounded, the tube bends in either the x or y direction.[19]

A piezoelectric actuator, as the name already implies, uses the piezoelectric effect, which causes a voltage, if mechanical stress is applied on a certain material [20]. But those materials exhibit the inverse effect as well, which is consequently called the inverse piezoelectric effect. By applying a voltage to the material, it either expands or contracts, depending on the polarity of the bias voltage, wherefore piezoceramics are ideal for that purpose. Naturally the expansion depends on the shape and size of the used material. A common technique is to use a piezoelectric tube scanner which can be seen in image 11. In this case a lead zirconate titanate (PZT) tube is used of about 2 inch length. Under ambient conditions the expan-

sion is usually only in the order of a few micrometers, which is sufficient for a safe approach to the sample.

The shape of the piezotube is a hollow cylinder with 4 equally arranged quadrant electrodes at the outer surface and one continuous electrode on the inside surface. A potential difference between the inside and all the outside electrodes causes the tube to either expand or contract equally in the z-direction. The expansion in the z-direction is illustrated in image 11a). Mathematically the equation which describes the displacement in the z-direction can be expressed the following way [21]:

$$\Delta z = \frac{L}{w} d_{31} \Delta V \tag{21}$$

Where L is the length of the tube and w the width between the inner and outer diameter of the tube. d_{31} is a piezoelectric coefficient which changes with temperature and ΔV is the applied voltage. The dependence upon the piezoelectric coefficient on temperature can be seen in image 12. At room temperature a value of $\approx 250\times10^{-12}\frac{m}{V}$ for PZT-5H can be read out.

In order to obtain a change in the x- or y-direction, a voltage +V is applied to one of the outer electrodes and a voltage -V is applied to the opposite electrode, while the other electrodes are grounded. The result is an expansion of one quadrant electrode while the opposite contracts, what causes the tube to bend into one direction. This motion allows the microscope to scan in the lateral directions. The bending of the tube in one of the lateral directions can be seen in image 11b). Due to the bending of the tube, one achieves that the tip moves in the x- or y-direction, but is not completely orthogonal to the z-axis. This however, doesn't have a big effect on the resulting image. Moreover the computer program for the readout can

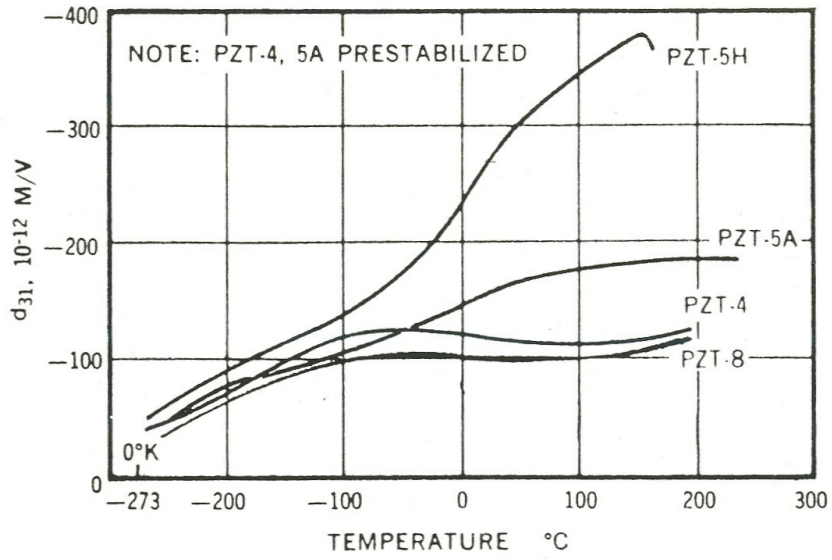

fig. 12: The piezoelectric coefficient is strongly dependent on the used material and temperature [12]

handle slopes of the surface and takes them into account for the image output. The equation which describes the motion of the tube in the x-y-direction is the following [21]:

$$\Delta x/y = \frac{2\sqrt{2}d_{31}VL^2}{\pi Dw} \tag{22}$$

Whereby d_{31} is the piezoelectric coefficient, V the applied voltage, L the length, D the diameter and w the width of the tube. In [21] the formula was derived without the factor "2" in the numerator. The reason for this factor in my equation is the fact that a voltage of a different polarity on two opposite electrodes is applied instead of only applying a voltage to one electrode while the opposite one is grounded, which constitutes another possibility to bend the tube. Therefore twice the bending can be obtained.

Apart from a piezotube, another piezoelectric element was used. Little Piezoplates with a length of 25 mm, a width of 5 mm and a thickness of only 0.3 mm were used for the approach process of the scanner tube to the sample. Due to their small height and width, the expansion in these directions, after applying a bias voltage, is negligible though. Only the length expansion plays an important factor. By applying an oscillating signal to the piezoplate, they expand and retract with a certain frequency. This property of the piezoplates will be used for moving the scanner tube up and down.

3.2.2 Moving the tube

As already mentioned, the smooth approach in small steps of the tip to the sample is a very crucial factor for a scanning tunneling microscope. There are several ways to approach the tip to the sample, for instance the piezoelectric stepper [4], the level motion demagnifier [22], the inchworm [23] or by using shear piezostack, as suggested by Pan [11] .

But in the scope of this master thesis we decided to use a modified version of the Pan type walker. This technique of moving the tube makes use of piezoplates which are attached to the T- and I-legs. At the loose end of the piezoplates a silicon pad is attached, which is in contact with 6 boron nitride pads being glued to the scanner tube. The principle how the tube is going to be moved is illustrated in figure 13 and is called "stick and slip" motion. In this image the walking process is illustrated with only 4 walkers instead of 6 but the principle is the same.

A high voltage is applied to the first piezoplate which causes an expansion of the piezoplate and the silicon pads, which is attached to the piezoplate, slips along the tube (step 1). It can slip, since the force it exerts on the tube is less than the force caused by the friction of the remaining legs which are at rest.

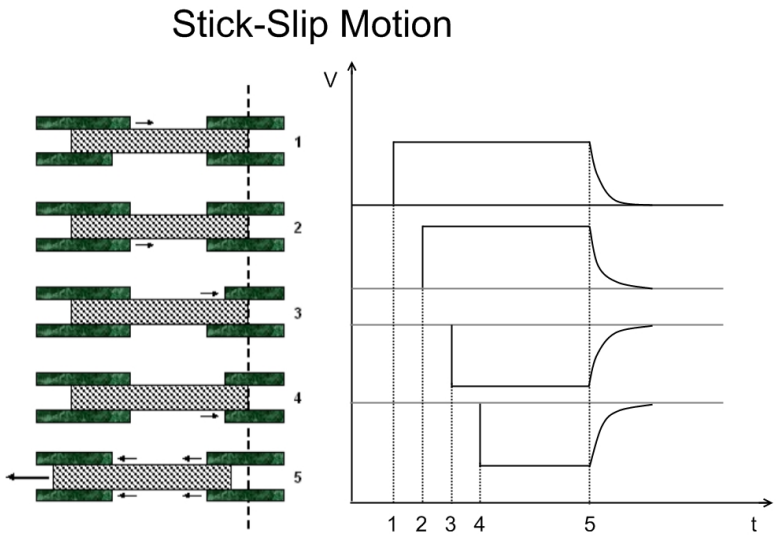

fig. 13: After applying a voltage successively to all the piezoplates, the voltage is cut and one step takes place [24][12].

The voltage which caused the expansion is kept up the whole time during one step, thus the silicon pad stays at the new position. After the first silicon pad has slipped along the tube and is at rest, the same voltage will be applied to the second piezotube (step 2). This process will be repeated with all the remaining piezoplates eventually (step 3,4). When every single silicon pad slipped along the tube, the voltage which kept the expansion of the piezoplates is cut (step 5). This engenders a moving step of the tube, since all the silicon pads return to their original position and pull the tube with them at the same time. The electrical circuit which had to be put together to achieve the desired signal can be seen in image 14.

The time delay, which is necessary, between the expansion of one piezoplate and the following can be achieved through the used relays. Due to its mechanical property the relay takes some time until it transfers the current to the next relay.

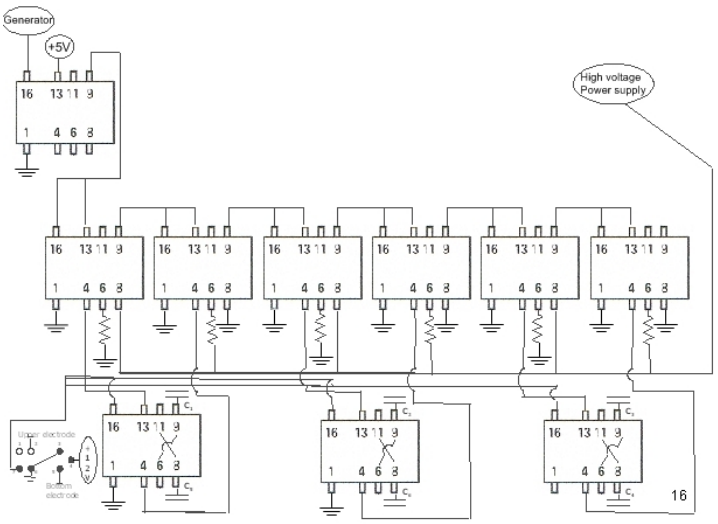

fig. 14: The relay on top is used to start one run. The six relays in the middle are used to apply the high voltage successively to the 6 piezoplates and the 3 relays at the bottom are used to switch the walking direction [24].

This time gap is sufficient for the silicon pads to slip along the tube while the others are at rest. The capacitors which are shown in image 14 at the 3 bottom relays illustrate the piezoplates.

3.3 Feedback loop

During the approach, one has to be sure, that the tip doesn't crash into the sample. Furthermore, after the coarse approach has taken place, one has to make sure that the tip keeps a constant distance to the sample, since the whole principle of the STM stands and falls with a constant gap distance. The whole theory is based on the fact that the tip can be stabilized at a desired distance from the sample. However, and due to thermal noise and vibrations, the tip usually changes its distance to the sample as time goes on. The fact that the tip rather moves around a certain position causes problems. Not having the tip at a stable position means,

one measures more or less random tunneling current and thus the image being taken of a sample would be random as well. A verification of the received data wouldn't be possible anymore. For that reason it is crucial to have vibrational isolation for the whole STM to obtain good images [27].
Moreover the distance between tip and sample is only in the order of a few nanometers, so the tip is always at risk of crashing into the sample, what has to be avoided by all means. Otherwise one has to replace the tip, since it has lost its tapered shape. Moreover the sample can be damaged. To avoid these issues one has to create a feedback loop which maintains the tunneling current and therefore the gap distance between tip and sample at a constant level. The principle of a feedback loop is clarified in image 15.

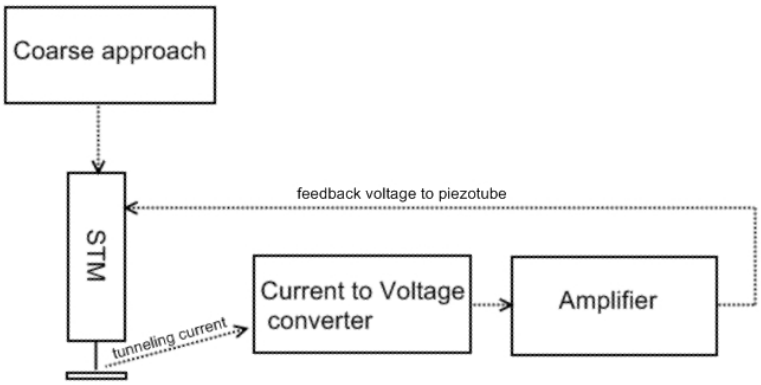

fig. 15: The tunneling current is amplified and converted into a voltage which in turn is used to control the gap distance between tip and sample.

By applying a small voltage between the tip and the sample, a tunneling current occurs which will be amplified. The amplified current is subsequently converted into a voltage signal. The closer the tip gets to the sample, the higher the tunneling current and the higher the voltage signal. This signal is consequently led into a second amplifier. The second amplifier subtracts the incoming voltage with a

priorly adjusted reference voltage. This reference voltage determines how far the tip can approach the sample. The higher the reference voltage, the smaller will be the distance between the tip and sample. Due to the property of subtraction of the reference and incoming voltage, the outcoming voltage of the amplifier applies a voltage to the piezotube in such a way that it withdraws the piezotube if the tip is too close (higher voltage signal than the adjusted one) or expands it, if the tip is too far away from the sample (smaller voltage signal than the adjusted one). Therefore one can achieve an equilibrium z-position and the gap distance is constant, since it is always compensated by a correcting voltage to the piezotube.

3.4 Scanning modes

3.4.1 Constant current mode

The most common mode of scanning the surface of a sample is the *constant current mode*. In this mode the tip rasters the surface of the investigated sample. The feedback loop, which is explained in section 3.3, hereby controls the gap distance between the tip and sample. If the measured tunneling current during one scan line turns out to be too small, the piezotube expands, which is triggered by the feedback loop, and brings the tip closer to the surface. If the tunneling current is too high, the tip is retracted. That means that the tip follows the corrugation of the sample's surface. The alternation in height, ΔZ, is monitored by a computer as a function of the X and Y position. By scanning an area line by line one obtains a topographic map of the sample.

3.4.2 Constant height mode

The *constant height mode* is the other possible mode of scanning a sample. As the name implies the tip rasters the surface at a certain height, rather than following

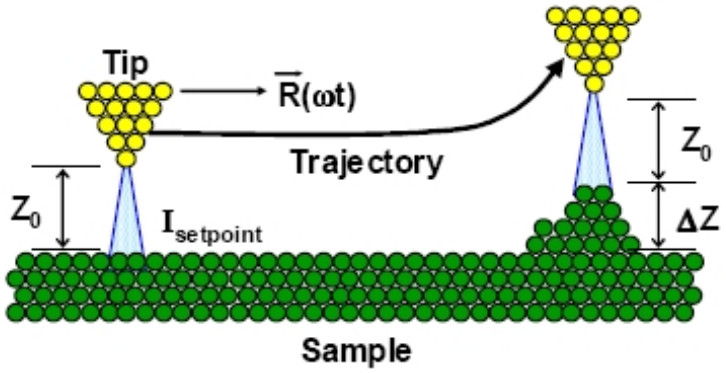

fig. 16: The tip rasters the surface in the constant current mode. ΔZ is measured and used for a topographic map [25].

the corrugation of the surface. In this case the tunneling current is used to create a topological map of the surface, since it is dependent on the tip-sample distance. However, this mode is rarely used, as it reveals a great disadvantage. If the tip doesn't follow the corrugation of the sample's surface, it might happen, that the tip "crashes" into protruding parts. Therefore the constant current mode is preferred, because it circumvents the problem neatly. On the other hand, if one is already aware of the investigated surface one can use this mode for a fast scan as in the *constant current mode* a certain time elapses for the new positioning of the tip, what makes this mode slower than the *constant height mode*.

3.5 Setup for the data acquisition

The last component which has to be considered is the data acquisition. In former times each line was scanned, subsequently printed on a sheet of paper and put together to obtain a topographic map of the scanned surface. A very famous example is the 7×7 unit cell of Silicon which can be seen in image 17 [1].

Nowadays a computer is used for the data acquisition. Image 18 illustrates the

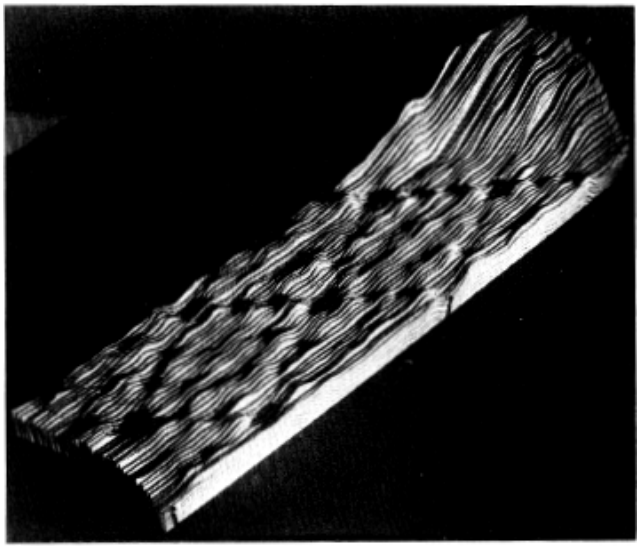

fig. 17: The 7×7 unit cell of Silicon is one of the first images ever taken by an STM, implemented by Binnig and Rohrer. Each single line of the rastered scan is clearly visible.[1]

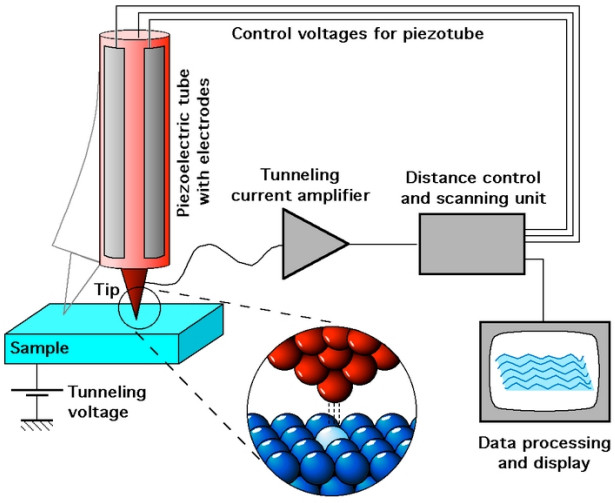

fig. 18: Schematic view of the whole STM setup. The feedbackloop is connected with a computer for the data acquisition. [26]

general principle of the setup which is necessary for the data acquisition. The microscope is on the one hand connected with the electrical circuit, described in section 3.2.2 which is responsible for the movement of the scanner tube. But on the other hand the tunneling current is connected with a readout device which in turn is connected with a data acquisition program on the computer. That means that every variable and component can be monitored and adjusted by the computer. When the STM rasters the surface of a sample, the change in ΔZ is measured and saved. Since the computer rasters the surface line by line, a topographic map of the surface can be obtained.

4 Assembly

Before the final assembly of the STM could be started, some preparations had to be done. 6 silicon pads had to be broken out of a wafer and ground into the desired size. As one side of the silicon pad isn't very smooth, it had to be treated with a micropolish powder since this side will have contact with the leg. Therefore the surface of the brass where the silicon pad will lay on top later on, has to be polished as well, to reduce the friction between the brass and the silicon pad. Apart from that 6 alumina tubes were cut and ground to fit into the designated hole of the leg (image 19). Epoxy was subsequently used to attach a small spring to the tube. These spring-loaded alumina tubes were put into the holes underneath the location where the piezoplates will be attached. A gold wire was put through the tube and bent on both sides so that the spring would push the gold wire later against the lower side of the piezoplate to achieve electrical conduction.

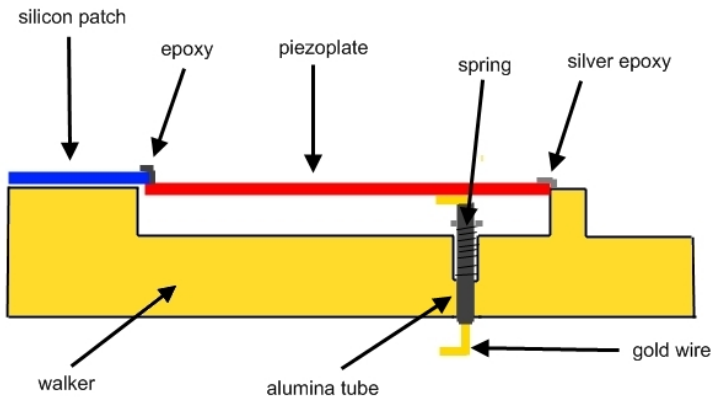

fig. 19: Schematic lateral view of the prepared leg.

After cleaning the piezoplates, they were attached to the legs. It is important that the piezoplates are only fixed on one side of the leg. If it had been fixed

on both ends, the expansion of the piezoplate which is necessary for the moving process while applying a voltage wouldn't have an effect anymore. Therefore, before hardening the epoxy on a hot plate, the leg was screwed into a certain appliance and the piezoplates had to be aligned carefully. Subsequently the silicon pads were attached to the loose ends of the piezoplates by using the same epoxy again. To achieve an electrical connection between the leg and the upper side of the piezoplate, a conductive silver epoxy was used to connect the upper side of the piezoplate electrically with the brass body. Image 19 illustrates a schematic view of the leg.

Apart from the 6 legs, the scanner tube had to be prepared as well. For that purpose the piezotube was glued on a prefabricated macor piece. The macor piece has 4 holes which are used to connect the 4 electrodes of the piezotube with strips of beryllium-copper. Furthermore one strip was glued to the inside of the piezotube to connect the inner electrode as well. Afterwards a little piece of delrin was rounded, cut to the length of about one inch, and glued on top of the piezotube. Since a small hole was drilled into the delrin piece before, a thin tipholder was stacked inside and glued with the delrin. This tipholder was connected with a wire to get a tunneling current later on. Now the macor piece with the piezotube on top could be glued to the brass tube. The complete assembled scanner tube is illustrated in image 20.

After having used epoxy again to attach 6 little boron nitride squares to the brass tube, the final assembly of the STM could be commenced.
The 4 T-walkers were screwed into the designated spots in the body. Subsequently the tube was eased into the body and the last two I-walkers were also screwed in. Each were springloaded at the lower part of the walker. The completely assembled

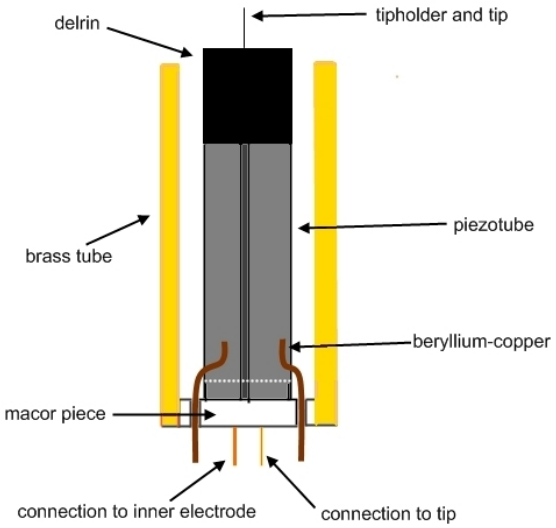

fig. 20: Schematic view of the scanner tube

body can be seen in image 21.
After having finished the body and the scanner tube, a sample holder was installed. Therefore three alumina rods were cut to a length of about 2“. These alumina rods are electrical isolating which is necessary to build up a potential difference between the sample and the tip. The alumina rods are stuck in the three holes at the top of the body and glued. The sample holder with its three holes can be put on the three alumina rods and be moved easily in the vertical direction. If one found the desired position, 3 screws were used to tighten the sample holder to the rods.

Several problems occurred during the assembly as well. If the small spring which was attached to the alumina tube wasn't at the right position, it either caused too big of a pressure to the gold wire and therefore to the piezoplate so that the plate was bent or, if the pressure was too low, the goldwire wasn't pushed against the plate at all. Therefore the right position of the spring at the alumina tube had to be found.

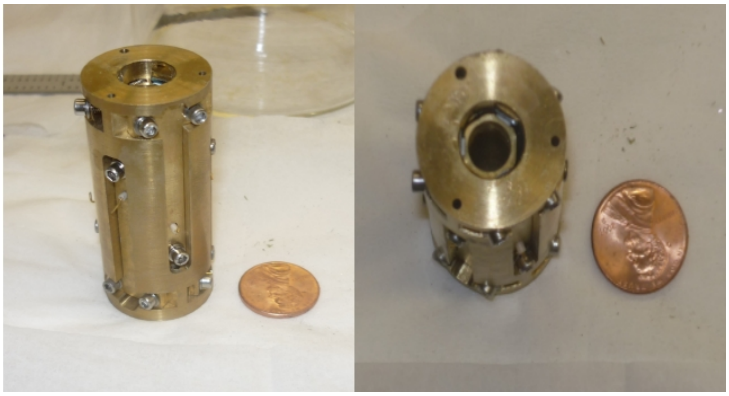

fig. 21: Completely assembled body of the STM.

Another posed problem was the fact that the piezoplates break very easily. One had to handle them very carefully. A lot of piezoplates broke while trying to screw the prepared walkers into the body. The reason was a small remnant of brass in the designated spots for the walkers, what caused the piezoplates to break while screwing the walker into the body.

5 Differences to older STM designs

Since the invention of the STM in 1986 by Binnig, a variety of different designs have been invented. Especially the ways to approach and scan the surface were subject to steady and continuous improvements.
This crucial part of the STM - the approach system - basically determines the whole design of the STM. Up to the present day, a lot of different approach systems were developed. Consequently I will only compare our used approach system, a modified version of the Pan-type positioner, on the one hand with an older system which is called the inchworm and on the other hand with the original pan-type walker.
What shouldn't go unmentioned is the fact that most of the approach systems have something in common - the use of the inverse piezoelectric effect. Very soon it was found out that this is a very promising method to approach the tip to the sample. It allows very small step sizes and is, furthermore, very reliable. Therefore making use of piezoelectric materials is popular for the approach system.

5.1 The Inchworm

One of the earliest inventions of an approach system is the inchworm [23] which was invented by Richard A. Bizzigotti at Burleigh Instruments Inc. in 1974. Originally it wasn't invented for the STM but it exhibits exactly the properties which can be used for an approach system in an STM. The inchworm has a very compact design and makes use of the inverse piezoelectric effect, too, as described in section 3.2.1.
It basically consists of 3 piezoceramic sections and a alumina shaft inside which can be seen in image 22. To perform a moving step, several steps are necessary.

At first one applies a voltage to the first section, which, as a consequence, clamps

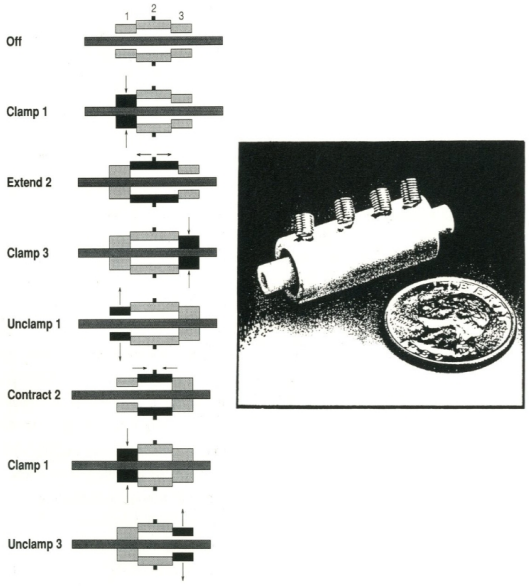

fig. 22: The inchworm and an illustration of the moving process [12].

to the alumina shaft. Subsequently, a voltage is applied to section 2 which has no contact with the alumina shaft and therefore expands its length. With the expanded section 2, a voltage is applied to section 3 to clamp to the shaft on his turn. By unclamping section 1 and contracting section 2 a small step was made alongside the alumina step.

The biggest disadvantage of the inchworm, is the fact, that everything has to be very precisely manufactured and assembled. Due to the small expansion of the piezoelectric ceramics, the alumina shaft has to be extremely straight, otherwise the clamping of the piezoceramics doesn't work and as a consequence the inchworm doesn't move anymore.

5.2 The Pan-type positioner

A big and noteworthy invention was done by S. H. Pan in 1993 [11].
The way, how the scanner tube is moved is illustrated in image 23. Pan made use of 4 shear piezostacks which surround the scanner tube. By applying a voltage to one of them, it deforms and slips alongside the tube while the other stacks and the whole scanner tube is at rest due to the friction exerted from the three remaining piezostacks. The slipped piezostack stays at its new position and a voltage is applied to the second piezostack. This step will be repeated to all of the legs. When all of the legs are at a new position, the voltage which kept them at the new position is ramped down and the piezostacks pull the scanner tube to a new position.
The new idea behind that moving process is the fact, that only one leg moves at a time and not several simultaneously.

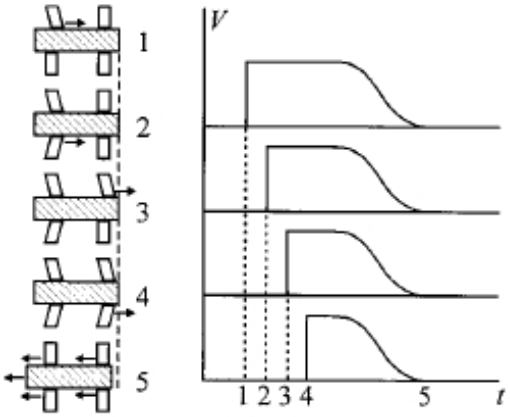

fig. 23: Illustration of the moving process suggested by Pan [28].

5.3 Modified Pan-type walking

Obviously the approach system being used by us extends the idea of Pan. The only difference between the original idea and our system is the fact, that we didn't use shear piezostacks, but piezoplates which slip alongside the tube and pull it to a new position.

5.4 Other differences

The history of STM has shown that the longer research is going on with STM, the more inventions and ideas arise, to make it more rigid and compact. In our case we managed it that the microscope could be more compact than previous designs. Mainly due to the use of piezoplates instead of shear piezostacks. By using piezoplates we could considerably reduce the diameter of the microscope. The microscope, described in [28] had a diameter of 1.5". In comparison, our microscope exhibits only a diameter of 1.0". This is advantageous, because the microscope becomes more practical to handle if one uses it in a cooling dewar, where space is limited.

Moreover this design exhibits another crucial property. It is simple to construct and the parts are, at large, easy to assemble. Moreover the approach system is easy to implement and very reliable, unlike the inchworm system, which relies on very precisely manufactured pieces.

6 Testing the microscope

6.1 Scanner tube movement tests

One of the first tests which were implemented were movement tests for the scanner tube, in order to check if the approach system works. For that reason the electrical circuit which was described in section 3.2.2 had to be put together and is illustrated in 14.

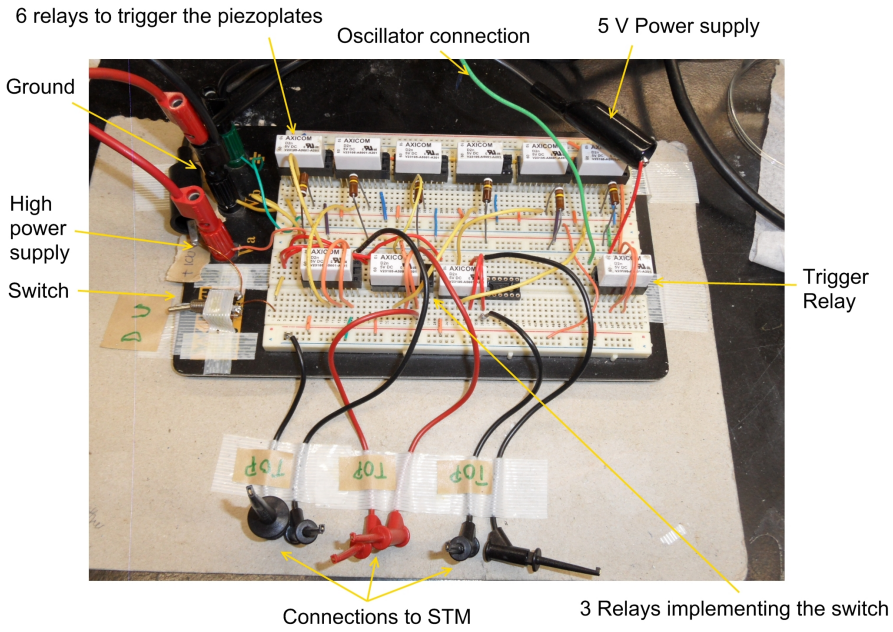

fig. 24: The electrical circuit, which was put together to create the signal to move the scanner tube either up or down.

The electrical circuit was put together on a simple breadboard. For the relays which serve as the time delay, 10 double pole double throw (DPDT) relays from *Axicom* were used. These relays can be driven with 5 V and have a release time of 4 ms which is sufficient for the time gap in between expanding the single piezoplates successively. Moreover a switch was built in the electrical circuit to easily change

the walking direction of the tube scanner. The complete put together electrical circuit can be seen in image 24.
To supply the power for the 10 relays with 5 V, a power supply from *Power design Inc.* was used. For the high voltage power supply which applies a voltage to the piezoplates, a *DC Power supply 9312 PS* was chosen. Furthermore the oscillator model *Wavetek 182 A* was chosen to provide the running signal.

In order to connect the electrical circuit with the microscope, 6 copper wires were prepared with a pin connector at one end. These ends are connected with the gold wires of the legs which in turn are connected with one electrode of the piezoplates. The other ends of the copper wires are simply connected with some clamps which were made for connection purposes between the electrical circuit and the STM.

For the first test a supply voltage of 100 V and a frequency of only about 2-3 Hz was chosen for the running signal. One has to keep in mind, that the frequency should not exceed a certain value. If so, it might happen that one moving step hasn't already finished while the following has already begun. As a consequence several piezoplates would expand simultaneously and a smooth walking of the scanner tube wouldn't be guaranteed anymore. Due to the fact, that the moving steps are fairly small, the movement of the scanner tube, seen with the naked eye, can only be noticed after 10-15 min.
An easy way, to check if the scanner tube moves, is to use a proximitor, in this case a *MicroPROX Sensor 5M-system* from *Bently Nevada*. By putting a metallic piece on top of the scanner tube and bringing it close to the proximitor, a voltage will be displayed. The alteration of the distance between the scanner tube and the proximitor consequently results in a voltage change of the proximitor. The proximitor which was used displayed a change of $\frac{2}{1000}\frac{V}{inch}$. Depending on the voltage

difference between one step, the step size can be calculated easily.
Most likely one couldn't find a setting at the beginning which allowed the scanner tube to move. Therefore one had to adjust the screws which push the beryllium-copper springs and which in turn push the I-legs against the scanner tube. This regulates the pressure exerted on the tube and thus effects the moving step size.
It turns out that the step size is between a few nanometers for low voltages and up to 1 μm for an applied voltages of about 100 V. Furthermore the testing of the moving was started with a high voltage of 100 V and was consequently reduced in order to find out the minimum voltage with which the scanner tube still moves. It turned out that this minimum voltage for my setup is around 25-30 V.

Another, even simpler, method was used as well, to determine the tube movement. A mirror was placed on top of the scanner tube under a crooked angle. A laser points laterally on the mirror and is reflected on a wall. If a correct setting is found and the tube starts moving, the mirror changes its angle and thus changes the position of the reflected laser point at the wall.
This technique is very simple and straight forward and is a quick way to check if the tube moves or not. Even the step size could be calculated by simple geometry. However, for determining the taken step size, a proximitor is certainly more precise.

It turned out that the 10 relays didn't have appropriate connections to be put into the breadboard. As a consequence they always hopped out, because of vibrations caused by the mechanical switching. A solution for that problem could be found by using adapters, which fit better into the breadbord so that the relays don't hop out.
Apart from that it always took a long time to find the correct adjustment of the force, caused by the screw which push the spring against the I-legs. If the I-legs

exert too little pressure on the tube, it is in danger of slipping. This requires a very careful handling with the adjustment of the screws. During the tests, the scanner tube slipped out of the body and it was so heavily damaged, that the whole scanner tube had to be opened and fixed again.

6.2 Testing the tunneling current

After making sure that the scanner tube is moving reliably, the first test with the STM could be done. Therefore a setup according to the feedback loop from section 3.3 was built up, which can be seen in image 25.

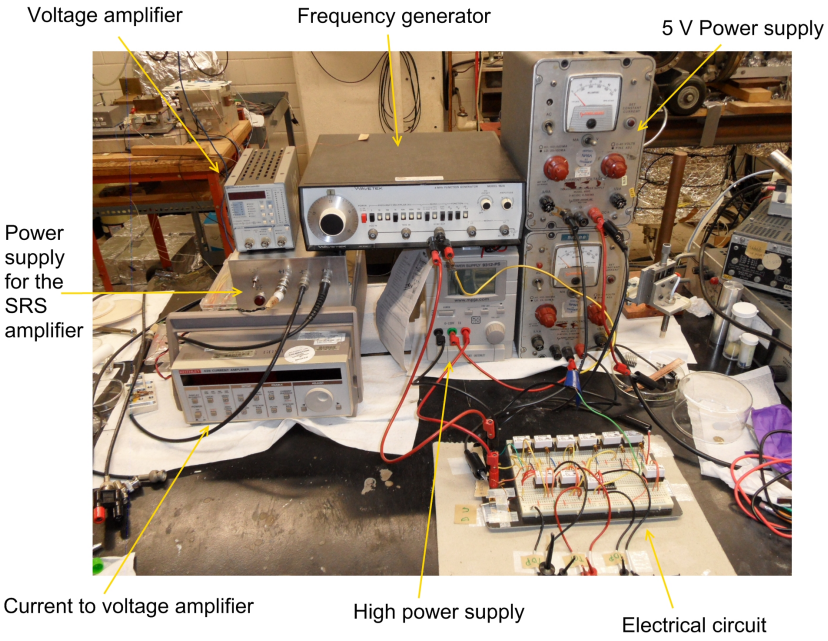

fig. 25: The setup for the first testings of the STM

To convert the tunneling current into a voltage, an amplifier from *Keithley 428 Current Amplifier* was used. The range of the possible amplification reached from

10^4 up to $10^{10}\frac{V}{A}$. The amplification which was used for the testings were $10^9\frac{V}{A}$. A typical value for a tunneling current is about 1 nA, what creates an output voltage of 1 V.

The output voltage was on the one hand connected with a voltmeter to monitor the tunneling voltage and therefore the distance between tip and sample and on the other hand connected with an amplifier from *Standford Research System, SIM 960 Analog PID Controller*. The output voltage of the SRS amplifier in turn was connected with the inner electrode and to the 4 outer electrodes of the piezotube, in order to provide the tube with a feedback signal. The STM was placed on top of a table which lacked the protection of vibrations, but it was sufficient for testing purposes. Moreover a voltage of 5 V was applied between the tip and the sample. However, to avoid a short between tip and sample, an additional resistance of 10 MΩ was put in between. Since the coarse approach of the tip to the sample had to be stopped manually, this of course involves the danger that the tip crashes into the sample and one has to replace it. To avoid ruining the new tip, an already used tip was used for the testings.

The coarse approach though, could be monitored with an ordinary microscope, to make sure, the tip has sufficient distance to the sample. If the distance became too small to be resolved by the ordinary microscope, the frequency of the taken steps was reduced to the possible minimum, which was 0.5 Hz. The reason for the reduction is only good measure. If the frequency of the steps being taken is too fast, it can happen, that the tip crashes into the sample before the operator is being able to react and stop the approach. Furthermore the changes in the tunneling current were better visible if the steps were taken more slowly.

After having approached the tip close enough to the sample, a tunneling cur-

rent eventually occurred which was converted into a voltage. Due to the fact that the feedback loop voltage is created by a subtraction of the tunneling voltage and a setpoint voltage of the *SRS* amplifier, the tip could be brought closer or further away from the sample by adjusting the setpoint voltage. The setpoint voltage could be fine adjusted up to 0.01 V. A stable position of a tunneling current could be achieved several times.

Unfortunately a problem occurred every time and couldn't be solved. The voltage displayed by the voltmeter was always circulating around a certain value. Therefore it was hard to get a stable tunneling position.
Furthermore it turned out that the voltmeter in this voltage setting could only display the measured voltage in 4 magnitudes. It happened many times, that a tunneling current outside of the detection of the voltmeter was measured, but when the next step was taken the tip had already crashed into the sample. A subsequent reduction of the supply voltage for the piezoplates which leads to a smaller expansion of the plates and thus to smaller step sizes didn't have the desired success.
For unknown reasons, a short occurred sometimes between the body and the lower electrode of the piezoplates. This demanded quite a lot of time to fix and replace it.

7 Data acquisition and first results

7.1 Data acquisition

After the microscope was tested for its functionality, the first images were taken. For that reason a setup according to section 3.5 was built.

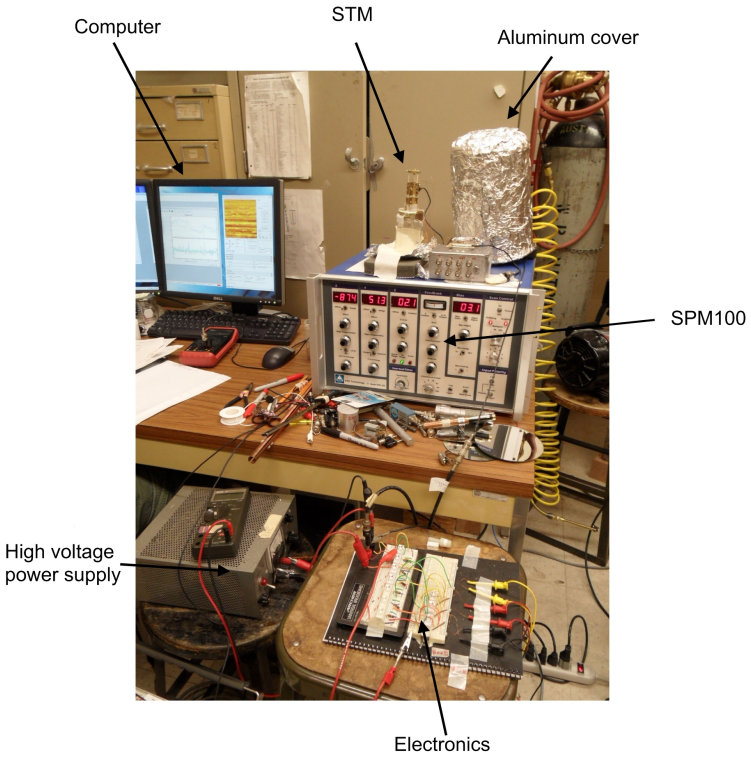

fig. 26: Setup for the scanning. The STM is connected with the electronics as well as with the SPM100 which in turn is connected with the computer. A simple foam was put underneath the STM for vibrational isolation. Moreover a glass covered with aluminum foil was used to block the STM off from interference radiation.

At first, the microscope was connected with the electrical circuit, described in section 3.2.2 which in turn is connected with the SPM100 and thus with the com-

puter. That means, that the approach can be completely monitored and controlled by the computer. In order to approach the tip to the sample, one adjusts a desired threshold tunneling current from the start. If the tunneling current eventually reaches this threshold value, the approach stops. It is advantageous that the piezotube is totally extended during the approach, because the tube can be easily and quickly retracted if reaching the threshold value so that a crash can be avoided if exceeding the value. If the tube hadn't been extended, a crash into the sample would have been possible, since this precaution wouldn't be ensured anymore, as one more moving step could easily cause a crash.

For the data acquisition, the XPMPRO^{TM} control software was used, which interfaces with the SPM100 electronics from RHK Technology [29]. It provides every feature necessary to scan and raster the sample. Furthermore it can display an instant image of the rastered sample, as every scanned line is being displayed immediately. This is advantageous as one can immediately stop the scan and delete the image, since one doesn't have to wait for the whole sample being scanned.
As seen on the image, the STM is underneath a glass, which is completely covered with aluminum foil. The purpose of this foil is the reduction of interference radiation. For that reason the connecting wires from the microscope to the electrical circuits were covered with aluminum foil as well. However, it turned out that the interference couldn't be totally screened.

7.1.1 HOPG

A very common sample for testing and calibrating STMs is HOPG (**H**ighly **O**rdered **P**yrolytic **G**raphite). Graphite is a very stable form of condensed carbon atoms which are sp^2-hybridized. The carbon atoms bond covalently and coplanarly to three other carbon atoms and thus form a hexagonal crystal structure. These σ-

bonds form a system of numerous layers which look like a honey comb, as can be seen in image 27.

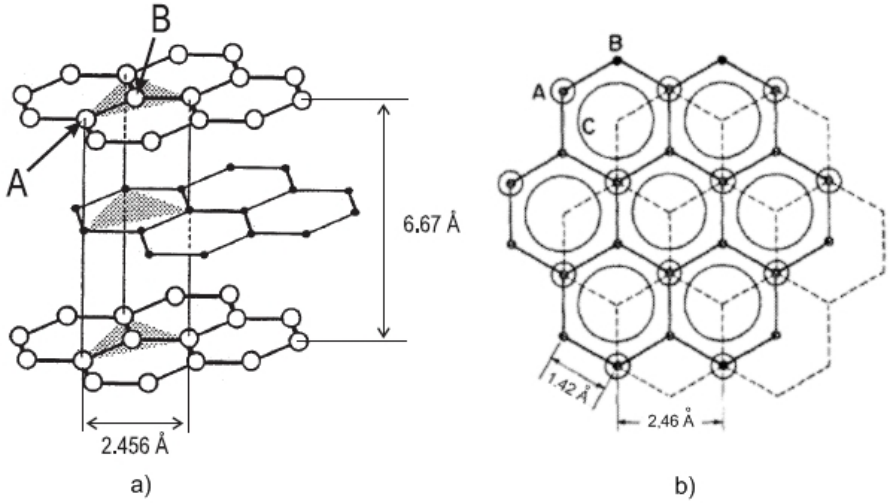

fig. 27: a) Crystal structure of HOPG [30]. b) The stacking sequence of graphite is ABAB, what has an effect on the LDOS at the A- and B-atom position. The solid line is the top layer, the dashed line represents the underlying layer [31].

The distance between two adjacent carbon atoms in one layer is 1.42 $\mathring{A}$ [31] and the lattice constant of a 2-atomic unit cell is about 2.46 $\mathring{A}$ [31]. Moreover the distance between two hexagonal shaped carbon layers is about 3.35 $\mathring{A}$ [30].
Two adjacent hexagonal shaped layers are bound weakly due to the *Van der Waals* force. This weak bonding and the anisotropy of the forces in different directions lead to very characteristic mechanical, electrical and thermal properties of graphite. Graphite, for instance, can easily be cleaved due to its weak bonding between the adjacent layers. One can use a simple adhesive tape to peel of the surface of graphite to obtain a clean and atomically flat sample. Furthermore the electrical and thermal conductivity is highly dependent on the orientation. Between the

two layers, graphite is almost electrically and thermally insulating, but it exhibits almost metallic conductivity alongside the plane [34].
The neighboring layers of graphite are shifted relatively to each other which results in an ABAB stacking sequence as shown in image 27b). Consequently there are two types of atoms, those with a direct neighbor in the adjacent layer (A-atoms) and those without a direct neighbor (B-atoms). Due to this atomic shift one can expect consequences in terms of the LDOS between an A- and a B-atom. This asymmetry of the LDOS near the Fermi energy of both atom positions was calculated by Tománek [32] in 1987. He showed that the electronic states at B-atoms are close to the Fermi edge, whereas the electronic states at the A-atoms form a continuum, which is spread over approximately 1.2 eV around the Fermi energy. Since the STM image is strongly dependent on the LDOS of a sample (see section 2.2), the B-atoms have a higher contribution to the tunneling current than A-atoms and therefore appear brighter. Besides, Tománek shows that this effect only decreases slightly with a higher tip-sample voltage.

Usually one uses synthetically produced HOPG instead of naturally occurring graphite. Natural graphite is too small and to difficult to obtain. HOPG, however, exhibits a big grain size, a lamellar structure [33] and, as the name already implies, it exhibits an angular spread between the graphite sheets of less than 1° [34]. Moreover HOPG is chemically inert to oxidation due to the lack of binding sites. Due to easy surface preparations and the high symmetry of HOPG, it is commonly used for STM or AFM calibration. The HOPG sample was illustrated together with the sample holder in image 9.

7.1.2 Scanning and results

The first real results with the STM were obtained by scanning a brass sample under ambient conditions. However, these results weren't really significant. It showed us though, that the readout with the computer and all the interfaces between the computer and the microscope work well together. Therefore we proceeded with the scan of a HOPG sample.

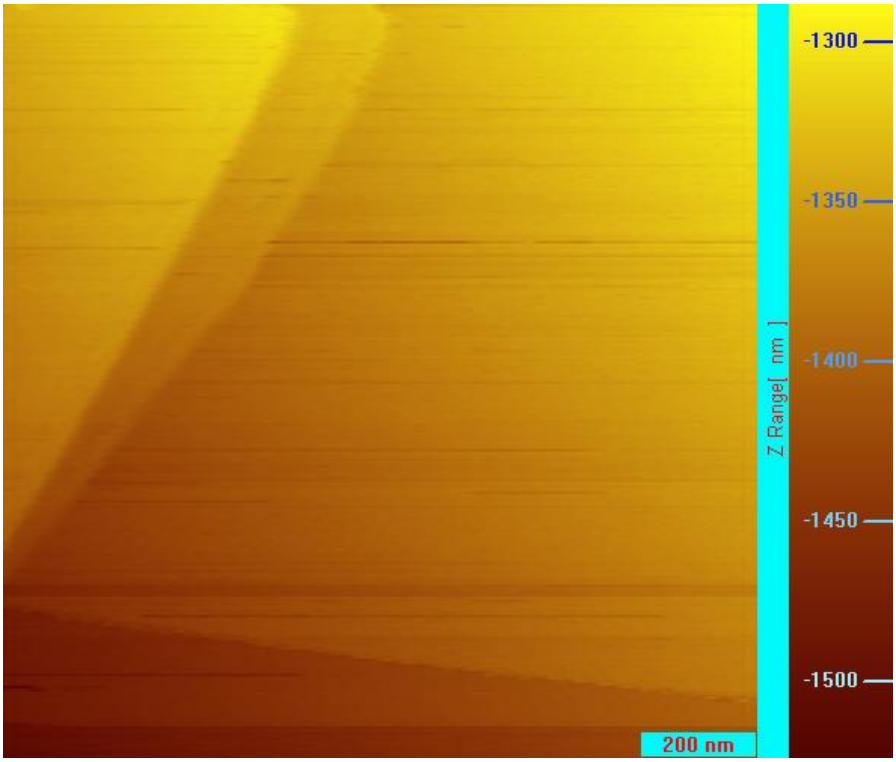

fig. 28: The scanned HOPG sample, 1.33 x 1.33 μm^2, U = 1 V and I = 0.28 nA. 3 clearly visible steps with a thickness of several layers cross the flat surface of the graphite sample.

The HOPG sample was scanned under ambient conditions and a simple foam underneath the STM was used as vibrational isolation, which can be seen in image

26. The result of the scanned graphite surface is illustrated in image 28.

The scanned area amounted to 1.33 x 1.33 μm^2. Apart from the plane surface which is clearly visible, one can also see 3 steps crossing the flat surface. By using the analyzing software, provided by RHK Technology, one can easily measure the step sizes. As can be seen on the image, the displayed image is crooked. In order to readout the step size it is reasonable to flatten the surface first. Afterwards one can use a simple cursor to determine the step size. It turns out that the left step is 30.07 nm thick, which corresponds to 9 graphite layers. The right step exhibits a thickness of 20.2 nm (6 layers), whereas the bottom one can be determined to a thickness of 23.71 nm (7 layers).

Attempts to get images of HOPG of higher resolution unfortunately failed or are of minor quality. Reasons for this failure exist in great numbers.
One likely reason might be (as already mentioned above) the unsuccessful screening of the STM from interference radiation. This resulted in a current which always interfered with the tunneling current and therefore affected the final result. This current didn't have a big effect on the large scaled image but could affect an image on a lower scale.
Furthermore the vibrational isolation was definitely not perfect, since we only used a foam underneath the STM which was fixed to the SPM100.
Moreover, problems with the tip can also never be completely excluded. Since real tips only exhibit an approximately tapered shape, they can always be a source of error.

For these reasons the images we tried to obtain in order to illustrate the hexagonal shape of HOPG either failed or were all blurred and not really meaningful.

8 Conclusion

In conclusion, a fully functioning scanning tunneling microscope has been constructed and assembled.

The STM has been machined in the student machine shop and was made out of brass.

After machining the pieces, they were cleaned, polished and assembled. Improvements in comparison to other STM designs were made for instance in terms of compactness. The microscope exhibits a diameter of only 1 inch, which makes it advantageous for the use in cooling devices. Pan's idea of moving the tube with piezostacks was further developed. Instead of piezostack, we used piezoplates which work very well and are very reliable.

Furthermore the electronics for the movement of the tube was put together. By contrast to formerly used electronics, where very elaborated and complex circuits had to be used, a more simplified but as effective circuit was used. The big difference depicts the use of relays, which provide, due to their mechanical functional principle, a sufficient long time gap between the single moving steps.

Subsequently the STM was tested on its functionality and first images of HOPG were taken under ambient conditions.

References

[1] G. Binnig, H. Rohrer, Ch. Gerber, and E. Weibel, *7×7 reconstruction on Si(111) resolved in real space*, Appl. Phys. Lett. 50, 120 1983

[2] G. Binnig, H. Rohrer, Ch. Gerber, E. Weibel, *Tunneling through a controllable vacuum gap*, Appl. Phys. Lett. 40 (1982), 178

[3] G. Binnig, H. Rohrer, Ch. Gerber, E. Weibel, *Surface Studies by Scanning Tunneling Microscopy*, Phys. Rev. Lett. 49 (1982), 57

[4] G. Binnig, H. Rohrer, *Scanning Tunneling Microscopy*, Helv. Phys. Acta, 55 (1982), 726

[5] G. Binning, C.F. Quate, *Atomic Force Microscope*, Phys. Rev. Lett. 56 (1986, 930-933)

[6] W. Häberle, J. K. H. Hörber, F. Ohnesorge, D. P. E. Smith, G. Binnig, *In situ investigations of single living cells infected by viruses*, Ultramicroscopy 42-44 (1992), 1161-1167

[7] L. Bartels, G. Meyer, K.-H. Rieder, *Basic steps of lateral manipulation of single atoms and diatomic clusters with a scanning tunneling microscope tip*, Phys. Rev. Lett. 79 (1997), 600

[8] G. Meyer, J. Repp, S. Zöphel, K.-F. Braun, S.W. Hla, S. Fölsch, L. Bartels, F. Moresco, K.-H. Rieder, *Controlled manipulation of atoms and small molecules with a low temperature Scanning Tunneling Microscope*, Single Mol. 1 (1) (2000), 25

[9] G. Meyer, S. Zöphel, K.-H. Rieder, *Controlled Manipulation of Atoms and Molecules and Formation of Nanostructures with the Low Temperature Scanning Tunneling Microscope*, Appl. Phys. A (1997), 31

[10] http://www.almaden.ibm.com/vis/stm/images/stm10.jpg

[11] S. H. Pan, International Patent Publication Number WO 93/19494 (International Bureau, World Intellectual Property Organization), 30 September 1993

[12] C. Julian Chen, Introduction to Scanning Tunneling Microscopy, Oxford University Press, 1992, ISBN: 0-19-507150-6

[13] http://en.wikipedia.org/wiki/Work_function

[14] J. Bardeen, *Tunneling from a many-particle point of view*, Phys. Rev. Lett. 6, 57 (1961)

[15] J. Tersoff and D. R. Hamann, *Theory and Application for the Scanning Tunneling Microscope*, Phys. Rev. Lett. 50, 25 (1983)

[16] J. Tersoff and D. R. Hamann, *Theory of the scanning tunneling microscope*, Phys. Rev. B, 31, 2 (1985)

[17] E. Stoll, A. Baratoff, A. Selloni and P. Carnevali, *Current distribution in the scanning vacuum tunnel microscope: a free-electron model*, J. Phys. C: Solid State Phys. 17 3073, 1984

[18] Drafts from Dr. Seong Heon Kim

[19] http://www.bostonpiezooptics.com/?D=8

[20] Ch. Kittel, Introduction to solid state physics, Wiley New York (1986)

[21] C. Julian Chen: *Electromechanical Deflections of Piezoelectric Tubes with Quartered Electrodes*, Appl. Phys. Lett., 1992, pp. 132-134

[22] D. P. E. Smith, G. Binning, *Ultrasmall scanning tunneling microscope for use in a liquid helium storage dewar*, Rev. Sci. Intrum. 57 (1986), 2630

[23] Richard A. Bizzigotti, Patent NOS 3902084, NOS 3902085, 25 November 1974

[24] Images created by Leu-Jen Chen

[25] Daniel Jay Hornbaker, *Electronic structure of carbon nanotube systems measured with scanning tunneling microscopy*, Thesis, University of Illinois at Urbana-Champaign, 2003

[26] http://en.wikipedia.org/wiki/File:ScanningTunnelingMicroscope_schematic.png

[27] M. Okano, K. Kajimura, S. Wakiyama, F. Sakai, W. Mizutani, M. Ono, *Vibration isolating for scanning tunneling microscopy*, J. Vac. Sci. Technol. A 5 (1987), 3313

[28] S. H. Pan, E. W. Hudson, and J. C. Davis, *3He refrigerator based very low temperature scanning tunneling microscope*, Rev. Sci. Instr. 70, (1999), 2

[29] XPMPRO manual

[30] R. Wiesendanger, Scanning Probe Microscopy and Spectroscopy, Cambridge University Press (1994)

[31] S.-I. Park, C. F. Quate, *Tunneling microscopy of graphite in air*, Appl. Phys. Lett. 48, 2 (1986), 112-114.

[32] D. Tománek, S. G. Louie, H. J. Mamin, D. W Abraham, R. E. Thomson, E. Ganz, J. Clarke, *Theory and observation of highly asymmetric atomic structure in scanning-tunneling-microscopy images of graphite*, Phys. Rev. B 35, 14 (1987, 7790-7793)

[33] http://www.2spi.com/catalog/new/hopgsub.php

[34] http://en.wikipedia.org/wiki/Graphite

[35] H. Chang, A.J. Bard *Observation and characterization by scanning tunneling microscopy of structures generated by cleaving highly oriented pyrolytic graphite*, Langmuir 7, 6 (1991, 1143-1153)

[36] G. Meyer, *A simple low-temperature ultrahigh-vacuum scanning tunneling microscope capable of atomic manipulation*, Rev. Sci. Instr. 67 (1996), 2960

[37] D.M. Eigler, E.K. Schweizer, *Positioning single atoms with a scanning tunneling microscope*, Nature 344 (1990), 524

[38] Y. Hasegawa and Ph. Avouris, *Manipulation of the Reconstruction of the Au(111) Surface with the STM*, Science 1992, Vol. 258 no. 5089 pp. 1763-1765